2,1,3-BENZOCHALCOGENADIAZOLES: REGULARITIES AND PECULIARITIES OVER A WHOLE CHALCOGEN PENTAD O, S, Se, Te AND Po

DOI: http://dx.medra.org/10.17374/targets.2020.23.143

Elena A. Pritchina[a,b], **Nina P. Gritsan**[a,c], **Oleg A. Rakitin**[d,e], **Andrey V. Zibarev***[c,f,g]

[a]*Institute of Chemical Kinetics and Combustion, Siberian Branch, Russian Academy of Sciences, 630090 Novosibirsk, Russia*

[b]*Department of Natural Sciences, Novosibirsk State University, 630090 Novosibirsk, Russia*

[c]*Department of Physics, Novosibirsk State University, 630090 Novosibirsk, Russia*

[d]*Institute of Organic Chemistry, Russian Academy of Sciences, 119991 Moscow, Russia*

[e]*Nanotechnology Education and Research Center, South Ural State University, 454080 Chelyabinsk, Russia*

[f]*Institute of Organic Chemistry, Siberian Branch, Russian Academy of Sciences, 630090 Novosibirsk, Russia*

[g]*Department of Chemistry, Tomsk State University, 634050 Tomsk, Russia*

(e-mail: zibarev@nioch.nsc.ru)

Abstract. *With DFT calculations, compared where possible with experimental data, molecular and electronic structure of the title compounds* ***1-5*** *(chalcogen=O, S, Se, Te and Po, respectively) and their radical ions was studied towards identification of regularities and peculiarities over a whole chalcogen pentad. Calculated properties of neutral molecules covered their geometries, atomic charges, bond orders and QTAIM descriptors, shapes and energies of π-MOs, ionization energy and electron affinity, NICSs, and MEPs; and those of radical ions included geometries, shapes and energies of π-SOMOs, electron spin density distributions, hyperfine coupling constants and g factors. In the most cases uniform patterns were obtained featuring only some particular peculiarities regarded to a certain chalcogen. The most important findings embrace reduced aromaticity of the heterocycles of* ***4*** *and* ***5*** *(NICS) and enlarged electrostatic contribution to their X–N bonds (QTAIM; X=Te, Po) as compared with* ***1-3****. However, the ground-state patterns are not enough to explain known differences in heteroatom reactivity of the title compounds. It is suggested that the differences come mainly from reaction kinetics and thermodynamics where widely varied atomic dipole polarizability of the chalcogens should be essentially important.*

Contents

1. Introduction

Chalcogen-nitrogen chemistry, especially heterocyclic, is an important part of contemporary main group chemistry including applications to material science and biomedicine.[1-6] In a fundamental aspect, however, a missing link is generalization covering all chalcogen pentad O, S, Se, Te and Po. The main reasons of this are enormous structural diversity of the chalcogen-nitrogen compounds and a lack of data on Po derivatives never studied experimentally due to radioactivity of the element.

In this situation, 2,1,3-benzochalcogenadiazoles (Scheme 1), relatively small and structurally-rigid 10π-electron hetero-analogs of naphthalene, seem to be a reasonable choice to begin discussion. Notably, these π-heterocyclic compounds are redox-active[7,8] and possess Lewis ambiphilicity.[6] The latter is dualistic in the sense that in both basic and acidic properties both π- and σ-MOs are involved, which is rather rare and can be used in various applications.[6] Overall, chemistry of O,[2,4] S[2,4-6,9,10] and Se[2,4-6] derivatives is well studied over more than a century, whereas that of Te congeners only emerges[5,6,8,11] and chemistry of Po ones does not exist. Due to this, the general discussion can only be based on computational results compared, where possible, with experimental data.

In this work, molecular and electronic structure of the archetypal 2,1,3-benzochalcogenadiazoles **1-5** (Scheme 1) and their radical ions was studied by means of DFT calculations. The radical ions are of special

interest as potential building blocks of functional magnetic materials. Calculated properties of neutral molecules covered their geometries, atomic charges, bond orders and QTAIM topological descriptors, shapes and energies of π-MOs, ionization energy and electron affinity, NICSs, and MEPs; and those of radical ions included geometries, shapes and energies of π-SOMOs, electron spin density distributions, hyperfine coupling (hfc) constants and g factors. In the most cases uniform patterns were obtained featuring only some particular peculiarities regarded to a certain chalcogen. The most important findings embrace reduced aromaticity of the heterocycles of **4** and **5** (NICS) and enlarged electrostatic contribution to their X–N bonds (QTAIM; X=Te, Po) as compared with **1**-**3**. However, the ground-state patterns are not enough to explain known differences in heteroatom reactivity of the title compounds. It is suggested that the differences come mainly from reaction kinetics and thermodynamics where widely varied atomic dipole polarizability of the chalcogens should be essentially important.

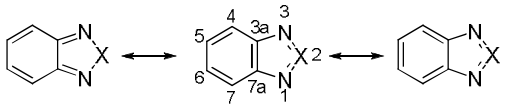

Scheme 1. 2,1,3-Benzochalcogenadiazoles **1**-**5** represented by superposition of quinoid (left) and benzenoid (middle and right) forms, X=O (**1**), S (**2**), Se (**3**), Te (**4**) and Po (**5**), and their atom numbering.

Unless otherwise indicated, the DFT calculations were performed with full optimization of molecular geometries with the *Gaussian09*[12] program package at the (U)B3LYP level of theory with the def2-tzvp basis set (for compounds **4** and **5** with ECP accounting 24 valence and 28 core electrons for Te atom, and 24 valence and 60 core electrons for Po atom). In all cases, the stability of the ground-state wave functions was verified.[13] Natural population analysis was carried out with the *NBO6* program (version for *Gaussian*).[14] The Mayer bond orders, MEPs, electron spin densities and QTAIM descriptors were obtained with the *Muliwfn 3.6* program.[15,16] Visualization was achieved with the *Chemcraft* program.[17]

2. Neutral molecules

For compounds **1**-**4**, XRD structures are known, the molecules are planar and feature C_{2v} symmetry slightly perturbed by crystal packing.[18-21] The DFT calculations reproduce the XRD geometries pretty well (Table 1).

Table 1. Bond lengths (Å) and bond angles (°) in heterocycles of compounds **1**-**5**.

Comp.	X	Method	Bond length			Bond angle		
			X–N	N–C	C–C[a]	N–X–N	X–N–C	N–C–C
1	O	XRD[18]	1.377, 1.391	1.303, 1.316	1.427	111.9	104.5, 105.0	108.8, 109.9
		B3LYP	1.362	1.316	1.432	113.1	104.8	108.6
2	S	XRD[19]	1.614, 1.620	1.348, 1.352	1.441	101.1	106.4, 106.5	112.8, 113.3
		B3LYP	1.615	1.341	1.443	101.1	106.4	113.1
3	Se	XRD[20]	1.777, 1.792	1.321, 1.328	1.437	94.7	106.8, 106.3	116.9, 116.3
		B3LYP	1.791	1.324	1.460	94.7	106.4	116.3
4	Te	XRD[21]	1.987, 2.014	1.314, 1.322	1.458	83.7	109.3, 112.2	115.2, 119.5
		B3LYP	1.986	1.317	1.478	88.1	106.8	119.1
5	Po	B3LYP	2.096	1.317	1.488	84.6	107.1	120.6

[a]Bond C3a–C7a in Scheme 1. Calculated lengths of bonds C3a–C4 (C7–C7a) and C5–C6 (Scheme 1) are 1.417-1.441 Å, and bonds C4–C5 (C6–C7) 1.355-1.367 Å. At the same level of theory, length of C–C bond in benzene is 1.391 Å.

The QTAIM[22] topological descriptors such as electron density ρ_b, its Laplacian $\nabla^2\rho_b$, and ratio of potential V_b and kinetic G_b energy densities at bond critical points suggest predominantly covalent X–N bonding in **1**-**5**, with some contribution of electrostatic interactions in **3**-**5** increasing with the atomic number Z of the chalcogen (Table 2).

Polarization of NXN fragment, as represented by natural atomic charges,[25,26] is very different for **1** and **2**-**4** where it is practically uniform (Table 3). Mayer bond orders[27] of X–N bonds in **1**-**5** suggest practically

single bonds (Table 3). This, together with the bond lengths (Table 1) implies dominance of the quinoid form in its superposition with the benzenoid form (Scheme 1). However, these findings cannot be taken without additional consideration since π-bonding situation in **1**-**5** is very special (for the initial discussion, see ref. 28). In all compounds p-AOs of the chalcogen and nitrogen atoms participate in the formation of the united π-system of molecule but contribute predominantly to π-MOs of different symmetry, *i.e.* to b_1 and a_2 MOs, respectively (Figure 1). Of five occupied π-MOs, chalcogen and nitrogen p-AOs are involved simultaneously only in the HOMO-4 in **1**-**3** and HOMO-3 in **2**-**4**, whereas in **5** there are no such MOs (designations HOMO-n regards only to Figure 1 but not to MOs' actual numbering). As a result, despite the chalcogen and nitrogen atoms of **1**-**5** jointly participate in the united π-systems of the molecules, π-density in the X–N bonds is low, which explains their low Mayer bond orders and long bond distances.

Table 2. QTAIM topological descriptors of X–N and N–C bonds in compounds **1**-**5**.[a]

Compound	X	Bond	ρ_b	$\nabla^2\rho_b$	$\lvert V_b\rvert/G_b$
1	O	O–N	0.346	–0.434	2.450
		N–C	0.369	–1.147	2.871
2	S	S–N	0.247	–0.240	2.245
		N–C	0.342	–1.071	3.051
3	Se	Se–N	0.188	0.010	1.982
		N–C	0.355	–1.119	2.973
4	Te	Te–N	0.143	0.200	1.594
		N–C	0.361	–1.146	2.968
5	Po	Po–N	0.126	0.210	1.493
		N–C	0.368	–1.162	2.920

[a]$\nabla^2\rho_b$ and ρ_b are given in au. For shared (*i.e.* covalent) bonding $\rho_b>0.2$, $\nabla^2\rho_b<0$, and $|V_b|/G_b>2$; for closed-shell (*i.e.* predominantly electrostatic) bonding $\rho_b<0.1$, $\nabla^2\rho_b>0$, and $|V_b|/G_b<1$.[23,24]

Table 3. Natural atomic charges and Mayer bond orders[a] in heterocycles of compounds **1**-**5**.

Comp.	X	Atomic charge			Bond order		
		X	N	C	X–N	N–C	C–C[b]
1	O	–0.093	–0.075	0.059	1.042	1.642	1.121
2	S	0.929	–0.601	0.092	1.349	1.494	1.139
3	Se	0.920	–0.597	0.094	1.254	1.588	1.073
4	Te	1.056	–0.661	0.096	1.191	1.638	1.028
5	Po	1.003	–0.628	0.093	1.154	1.730	0.986

[a]The values of Mayer bond orders are in agreement with empirical ones to be close to 1.0, 2.0 and 3.0 for single, double and triple bonds, respectively. At the same level of theory, Mayer bond order of C–C bond in benzene is 1.418. [b]Bond C3a–C7a in Scheme 1.

Notably, whilst the LUMOs of **1**-**5** are isolobal, the HOMOs are not as the HOMO of **5** is different from those of **1**-**4** (Figure 1). On going from **1** to **5**, the energy gap between the frontier MOs monotonically decreases (Figure 1), which correlates with bathochromic shift of the long-wavelength absorption band in experimental UV-Vis spectra of **1**-**4** (Figure 2).

The first ionization energy (IE_1) of **1**-**4** is less sensitive to the nature of chalcogen (Table 4), which can be explained via the Koopmans theorem by a lack of chalcogen contribution to their HOMOs of a_2 symmetry (Figure 1). Calculated adiabatic IE_1 of **5** also fits this pattern. DFT predicts for **5** practically degenerated HOMO and HOMO-1 of b_1 and a_2 symmetry, respectively, with the HOMO featuring significant contribution from Po (Figure 1). Overall, slight decrease of IE_1 in the series **1**-**5** correlates with decrease of electronegativity (EN)[29] of the chalcogen atoms.

DFT-calculated first adiabatic electron affinity (EA_1) of **1**-**5** is positive (Table 4), which means that their radical anions (RAs) are thermodynamically more preferable than neutral molecules.[30-32] Due to this, compounds **1**-**5** are efficient electron acceptors, and **1**-**3** and their derivatives found numerous relevant applications in both chemistry and materials science (available literature is too abundant to be cited

completely, for introduction see refs. 2, 4-6, 9, 33,34 and refs. therein). Notably, EA_1 in the series **1**, **3**-**5** and **2**-**5** increases with Z of the chalcogen (Table 4), which, in contrast to the situation with IE_1, contradicts EN[29] of the chalcogens. For **2**-**4** this trend is experimentally confirmed by electrochemical data.[7,8,30,35-37] Tentatively, the trend can be explained by better charge / spin delocalization in diffuse π-SOMOs of RAs containing contribution from heavier chalcogens. For **1** and **2**, higher EA_1 of the former can be associated with higher EN[29] of O as compared with S.

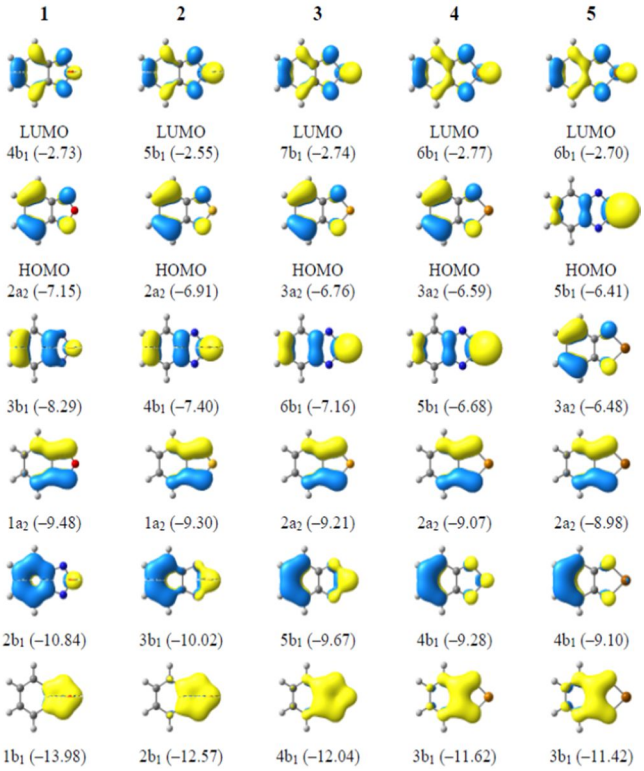

Figure 1. The LUMO, HOMO and four other occupied π-MOs of compounds **1**-**5**, and their energies (eV).

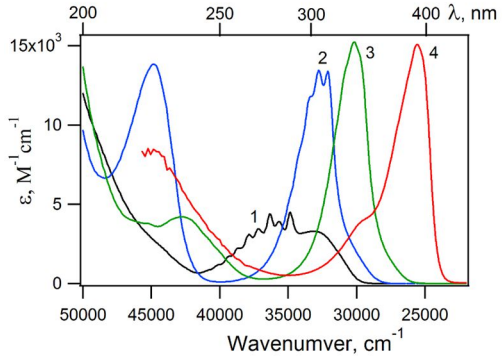

Figure 2. Experimental UV-Vis spectra of compounds **1**-**3** in ethanol and **4** in THF.

Table 4. IE_1 and EA_1 of compounds **1-5** (eV).[a,b]

Compound	X	EN[c]	IE_1		EA_1
			He(I) PES	B3LYP	
1	O	3.61	9.37;[38] 9.58[39]	9.09 (9.05)	0.93 (1.04)
2	S	2.59	8.95;[40] 8.98;[38,41] 9.00[39,42,43]	8.74 (8.70)	0.82 (0.92)
3	Se	2.42	8.76;[43] 8.80;[41] 8.81[39]	8.53 (8.50)	1.02 (1.11)
4	Te	2.16	8.57[41]	8.26 (8.22)	1.12 (1.20)
5	Po	2.19	–	8.10 (8.07)	1.10 (1.19)

[a]Values in brackets obtained with ZPVE correction. [b]Measured IE_1 are vertical, whereas calculated adiabatic. [c]The Allen scale in Pauling units.[29]

Magnetic descriptor NICS[44-46] suggests aromaticity[47] of carbocycles of compounds **1-5**, which slightly depends on the nature of chalcogen atoms. The NICS values of heterocycles are more chalcogen-dependent and notably lower those of the carbocycles. For **4** and **5**, the NICS(0) values imply situation with conjugated non-aromatic rather than aromatic heterocycles (Figure 3). It can be explained by worse overlap between 2p-AO of N with 5p-AO of Te and 6p-AO of Po as compared with np-AOs (n=2-4) of the lighter chalcogens. Despite NICS is magnetic criterion, the aromaticity is basically thermodynamic conception[47] and reduced aromaticity means reduced thermodynamic stabilization caused by perimeter delocalization of π-electrons in a π-conjugated cyclic system. In the context of heteroatom reactivity, reduced aromaticity of the heterocycle of **4**, *i.e.* its reduced thermodynamic stabilization, should influence accessibility of certain transitions states (TSs) as compared with **1-3** (see below).

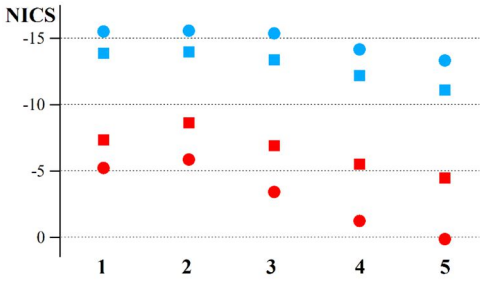

Figure 3. NICS(0) and NICS(1) values (circles and squares, respectively) for carbo- (blue) and hetero- (red) cycles of **1-5**. At the same level of theory for benzene, the NICS(0) and NICS(1) are –8.11 and –10.03, respectively.

MEPs[48] of compounds **1-5** reveal σ-holes,[49-51] *i.e.* regions of poor electron density/positive electrostatic potential (Figure 4), associated with the chalcogens and arising from the anisotropy of the atomic charge distributions.

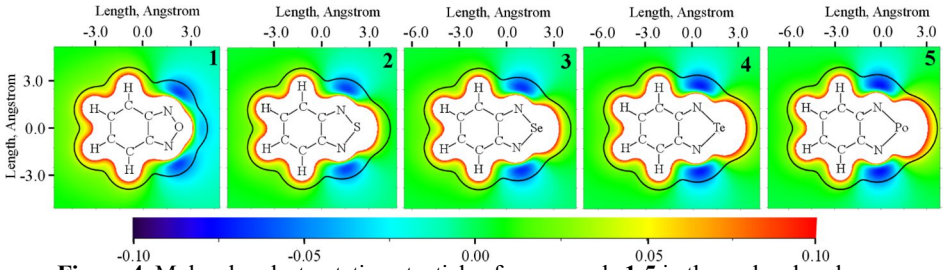

Figure 4. Molecular electrostatic potentials of compounds **1-5** in the molecular planes, black curves correspond to the electronic density ρ=0.001 au.

The σ-holes are important for ability of **1**-**5** to participate in secondary bonding interactions (SBIs),[52] which are more pronounced with heavier chalcogens. The SBIs, particularly, include chalcogen bonding, *i.e.* the attractive interactions between chalcogen sites in molecules and Lewis bases/nucleophiles,[53] in the case of **2**-**4** and related chalcogenadiazoles.[6,8,11,54-61] In the solid state, these SBIs manifest themselves in the shortened intermolecular contacts X…N (X=S, Se, Te) leading to supramolecular association, which can be used in crystal engineering.[11,54] Compound **1** is unstudied in this context although O derivatives can, principally, be involved in the chalcogen bonding, at least in the solid state.[53]

3. Radical anions

RAs of compounds **1**-**3** are known with solution EPR since 1965,[62] whereas that of **4** only since 2019.[8] As compared with EPR spectrum of $[\mathbf{3}]^{\cdot-}$, that of $[\mathbf{4}]^{\cdot-}$ features broadened lines and is significantly g-shifted (Figure 5) due to stronger spin-orbit coupling (SOC) at the Te atom than at the Se atom[8] (the strength of the SOC increases sharply as Z^4 to be efficient for atoms with Z>30;[63,64] for O, S, Se, Te and Po, Z=8, 16, 34, 52, and 84, respectively). The SOC is important for molecular magnetism in the solid state since it can be involved in spin canting leading to ferromagnetic (FM) ground state of a substance under conditions of antiferromagnetic (AF) exchange interactions between its paramagnetic centers.[65-67]

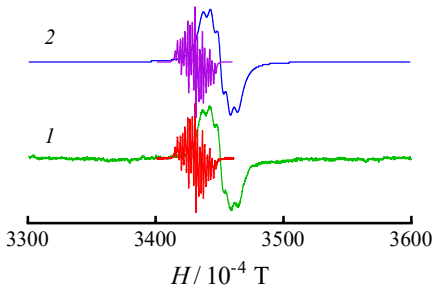

Figure 5. EPR spectra of $[\mathbf{3}]^{\cdot-}$ (red and violet lines) and $[\mathbf{4}]^{\cdot-}$ (green and blue lines) featuring shift of g factor (*1*–experiment, *2*–simulation).[8]

DFT-calculated π-SOMOs of $[\mathbf{1}]^{\cdot-}$-$[\mathbf{5}]^{\cdot-}$ are isolobal (Figure 6), and electron spin density distribution in these RAs is quite uniform (Figure 7, Table 5).

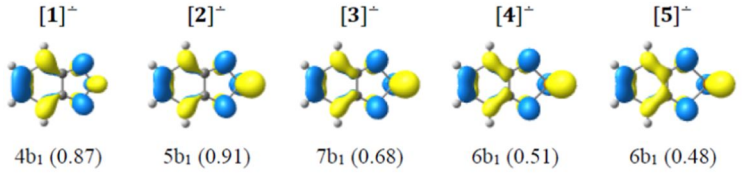

Figure 6. π-SOMOs of $[\mathbf{1}]^{\cdot-}$-$[\mathbf{5}]^{\cdot-}$ and their energies (eV).

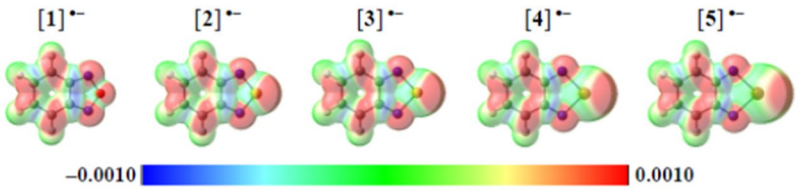

Figure 7. Electron spin density distribution on the VdW surfaces of $[\mathbf{1}]^{\cdot-}$-$[\mathbf{5}]^{\cdot-}$.

Table 5. Atomic spin populations in [**1**]$^{\cdot-}$-[**5**]$^{\cdot-}$ from DFT calculations.

RA	X	Atom				
		X2	N1, N3	C3a, C7a	C4, C7	C5, C6
[**1**]$^{\cdot-}$	O	0.161	0.250	–0.062	0.193	0.055
[**2**]$^{\cdot-}$	S	0.252	0.237	–0.047	0.151	0.046
[**3**]$^{\cdot-}$	Se	0.199	0.271	–0.037	0.129	0.049
[**4**]$^{\cdot-}$	Te	0.168	0.287	–0.025	0.113	0.051
[**5**]$^{\cdot-}$	Po	0.127	0.304	–0.023	0.113	0.054

On the van der Waals (VdW) surfaces of the RAs the density is mainly positive with only small islands of negative values in the area of the C3a–C7a bond. Spin polarization is a real physical property which, similarly to the SOC, is important for molecular magnetism in the solid state: contacts between the like spin density of neighboring paramagnetic species lead to AF exchange interactions, whereas those between unlike density to FM interactions.[65]

The hfc constants of [**1**]$^{\cdot-}$-[**5**]$^{\cdot-}$ reveal weak dependence on the nature of chalcogen (Table 6); it follows from EPR data that UB3LYP/def2-tzvp calculations underestimate hyperfine coupling with nitrogen nuclei.

Table 6. Hyperfine coupling constants[a,b] (G) and g factors of [**1**]$^{\cdot-}$-[**5**]$^{\cdot-}$.

RA	X	Method	Hfc constant			g_{iso}
			N1, N3	H4, H7	H5, H6	
[**1**]$^{\cdot-}$	O	EPR[62]	5.24	3.33	2.02	–
		UB3LYP	3.88	–4.37	–1.73	2.0043
[**2**]$^{\cdot-}$	S	EPR	5.26;[62] 5.31[37]	2.63;[62] 2.61[37]	1.61;[37] 1.53[62]	2.00225[37]
		UB3LYP[c]	5.46	–3.81	–1.52	2.00288
		UB3LYP	3.90	–3.41	–1.44	2.0046
[**3**]$^{\cdot-}$	Se	EPR[37]	5.73	2.36	1.61	2.0064
		UB3LYP	4.20	–2.96	–1.47	2.0068
		DKH2-UB3LYP[d]	5.18	–2.98	–1.46	2.0076
[**4**]$^{\cdot-}$	Te	EPR[8]	5.85	–[e]	–[e]	1.9952
		DKH2-UB3LYP[d]	5.12	–2.67	–1.47	1.9947
[**5**]$^{\cdot-}$	Po	DKH2-UB3LYP[d]	5.01	–2.54	–1.52	1.9230

[a]Constants of isotropic Fermi contact coupling. [b]The calculations were performed using the *ORCA* 4.0.1 suit of programs with implemented version of UB3LYP.[68] [c]UB3LYP/6-31+G(d).[37] [d]All-electron calculations using the scalar relativistic DKH2 Hamiltonian[69] with DKH-def2-tzvp reconstructed basis sets[70] for C, H, N, Se and Te atoms, and SARS-DKH-def2-tzvp basis set[71] for Po atom. [e]No hfc constants were experimentally assessed due to the line broadening.

RAs [**2**]$^{\cdot-}$, [**3**]$^{\cdot-}$ and [**4**]$^{\cdot-}$ are isolated in the form of thermally-stable salts of cations $[K(THF)]^+$, $[K(18\text{-crown-6})]^+$ or $[K(18\text{-crown-6})(THF)]^+$ upon chemical reduction of **2**-**4** with elemental K, and characterized by XRD[8,72,73] and DFT (Table 7). In contrast to [**2**]$^{\cdot-}$ and [**3**]$^{\cdot-}$ isolated in the form of ordinary 1:1 cation/anion salts, [**4**]$^{\cdot-}$ was isolated in the form of 2:1 salt (Figure 8) whose dianion is formally composed of neutral molecule **4** and two RAs [**4**]$^{\cdot-}$ asymmetrically bound by Te…N contacts.[73] Broken-symmetry DFT calculations suggest the singlet ground state of this specie, *i.e.* $[\mathbf{4}_3]^{2-}$ (on singlet diradicals see ref. 74), caused by AF exchange interactions with J=–0.13 eV. More rigorous CASSCF calculations give J=–0.16 eV and suggest that the singlet ground state of $[\mathbf{4}_3]^{2-}$ contains 15% contribution of diradical character (details will be published elsewhere).[73] According to DFT calculations, the negative charge of $[\mathbf{4}_3]^{2-}$ is highly delocalized and it is impossible to distinguish between neutral and charged **4** units within the specie.

Structural changes on going from neural molecules (Table 1) to RAs (Table 5), particularly elongation of bonds X–N, correspond to nodal properties of the π-LUMOs of **1**-**5** (Figure 1)/π-SOMOs of [**1**]$^{\cdot-}$-[**5**]$^{\cdot-}$ (Figure 6).

Table 7. Bond lengths (Å) and bond angles (°) in heterocycles of $[\mathbf{1}]^{\bullet-}$-$[\mathbf{5}]^{\bullet-}$.

RA	X	Method	Bond length			Bond angle		
			X–N	N–C	C–C[a]	N–X–N	X–N–C	N–C–C
$[\mathbf{1}]^{\bullet-}$	O	B3LYP	1.415	1.328	1.444	111.5	104.5	109.7
$[\mathbf{2}]^{\bullet-}$	S	XRD[72]	1.665, 1.669	1.355, 1.370	1.439	99.8	106.0, 106.4	113.4, 114.4
		B3LYP	1.671	1.349	1.454	99.9	105.8	114.2
$[\mathbf{3}]^{\bullet-}$	Se	XRD[8 b]	1.813, 1.842; 1.829, 1.833	1.353, 1.362; 1.351, 1.354	1.435; 1.446	95.0; 94.9	104.8, 104.9; 104.9, 105.1	117.1, 118.2; 117.2, 117.9
		B3LYP	1.840	1.343	1.464	94.6	105.2	117.5
$[\mathbf{4}]^{\bullet-}$ [c]	Te	XRD[74]	2.019, 2.094; 2.036. 2.096; 2.034, 2.066	1.308, 1.314; 1.357, 1.360; 1.343, 1.349	1.479; 1.445; 1.467;	83.3; 81.2; 84.0	109.1, 110.4; 112.5, 111.3; 109.0, 110.2	117.9, 119.3; 116.5, 118.0; 117.9, 118.7
		B3LYP	2.023	1.343	1.474	88.7	105.3	120.3
$[\mathbf{5}]^{\bullet-}$	Po	B3LYP	2.134	1.338	1.481	85.4	105.4	121.0

[a]Bond C3a–C7a in Scheme 1. Calculated lengths of bonds C3a–C4 (C7–C7a) and C5–C6 (Scheme 1) are 1.410 ($[\mathbf{2}]^{\bullet-}$)-1.441 ($[\mathbf{5}]^{\bullet-}$) Å and 1.398 ($[\mathbf{2}]^{\bullet-}$)-1.406 ($[\mathbf{5}]^{\bullet-}$) Å respectively, and bond C4–C5 (C6–C7) 1.383 ($[\mathbf{5}]^{\bullet-}$)-1.398 ($[\mathbf{1}]^{\bullet-}$) Å. [b]Data for two salts of $[\mathbf{3}]^{\bullet-}$ with different cations. [c]See relevant text above.

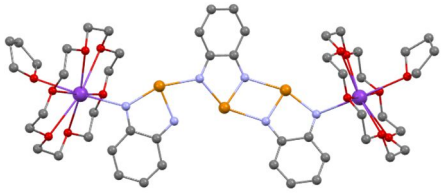

Figure 8. XRD structure of RA salt $[K(18\text{-crown-6})(THF)]_2[\mathbf{4}_3]^{2-}$.[73]

4. Radical cations

Radical cations (RCs) of compounds **1**-**3** were tried to access electrochemically but oxidation of neutral precursors was irreversible and neither target $[\mathbf{1}]^{\bullet+}$-$[\mathbf{3}]^{\bullet+}$ nor other paramagnetic species were detected by EPR.[7,37] This does not exclude attempts of chemical preparation of the RCs.

DFT calculated π-SOMOs of $[\mathbf{1}]^{\bullet+}$-$[\mathbf{5}]^{\bullet+}$ are isolobal (Figure 9) and correlate with the π-HOMOs of **1**-**5** (Figure 1). They do not contain contribution from the chalcogen atoms due to which their energies are rather invariant to the nature of these atoms (Figure 9).

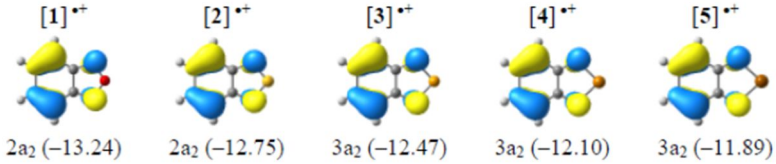

Figure 9. π-SOMOs of $[\mathbf{1}]^{\bullet+}$-$[\mathbf{5}]^{\bullet+}$ and their energies (eV).

Electron spin density distribution in $[\mathbf{1}]^{\bullet+}$-$[\mathbf{5}]^{\bullet+}$ (Figure 10, Table 8) reveals enlarged areas of negative values associated not only with bond C3a–C7a, as in $[\mathbf{1}]^{\bullet-}$-$[\mathbf{5}]^{\bullet-}$, but also with the chalcogen atoms. This provides better possibilities for FM exchange interactions between the RCs in the solid state and motivates chemical synthesis of their salts.

As in $[\mathbf{1}]^{\bullet-}$-$[\mathbf{5}]^{\bullet-}$ (Table 6), the DFT-calculated hfc constants in $[\mathbf{1}]^{\bullet+}$-$[\mathbf{5}]^{\bullet+}$ slightly depend on the nature of chalcogens (Table 9).

5. Conclusions

On the basis of DFT calculations performed in this work on isolated molecules of neutral 2,1,3-benzochalcogenadiazoles **1**-**5** and their radical ions and comparison of the results with relevant experimental data, no one element of group 16 can be claimed a *maverick among the chalcogens* (formulation is taken

from ref. 75) with possible exception for Te in the context of RAs (*i.e.* singlet diradical $[\mathbf{4}_3]^{2-}$ vs. $[\mathbf{2}]^{\cdot-}$ and $[\mathbf{3}]^{\cdot-}$).

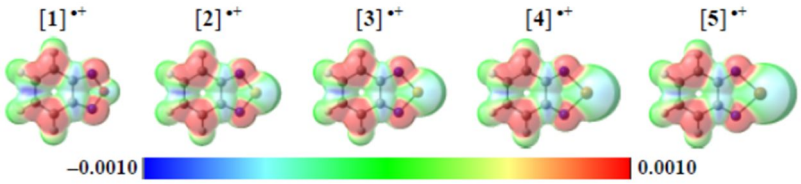

Figure 10. Electron spin density distribution on the VdW surfaces of $[\mathbf{1}]^{\cdot+}$-$[\mathbf{5}]^{\cdot+}$.

Table 8. Atomic spin population in $[\mathbf{1}]^{\cdot+}$-$[\mathbf{5}]^{\cdot+}$ from DFT calculations.[a]

RC	X	Atom				
		X2	N1, N3	C3a, C7a	C4, C7	C5, C6
$[\mathbf{1}]^{\cdot+}$	O	–0.042	0.227	–0.076	0.343	0.040
$[\mathbf{2}]^{\cdot+}$	S	–0.065	0.189	–0.061	0.370	0.049
$[\mathbf{3}]^{\cdot+}$	Se	–0.089	0.216	–0.068	0.358	0.053
$[\mathbf{4}]^{\cdot+}$	Te	–0.125	0.236	–0.070	0.351	0.059
$[\mathbf{5}]^{\cdot+}$	Po	–0.151	0.255	–0.072	0.344	0.063

[a]The instability of the RCs' wave functions under perturbation was observed, and the reoptimization of the ground-state wave-functions to lower-energy solutions was performed using orbital rotation.

Table 9. Hyperfine coupling constants[a] (G) and g factors of $[\mathbf{1}]^{\cdot+}$-$[\mathbf{5}]^{\cdot+}$ from DFT calculations.[b-d]

RC	X	Hfc constant			g
		N1, N3	H4, H7	H5, H6	
$[\mathbf{1}]^{\cdot+}$	O	2.96	–7.66	–1.41	2.00270
$[\mathbf{2}]^{\cdot+}$	S	2.04	–8.25	–1.69	2.00254
$[\mathbf{3}]^{\cdot+}$	Se	2.22	–7.15	–2.10	2.00113
$[\mathbf{3}]^{\cdot+}$	Se[e]	2.91	–7.13	–2.11	2.00092
$[\mathbf{4}]^{\cdot+}$	Te[e]	2.88	–7.79	–1.92	1.99649
$[\mathbf{5}]^{\cdot+}$	Po[e]	2.89	–7.65	–1.99	1.97542

[a]Constant of isotropic Fermi contact coupling. [b]The calculations were performed using the *ORCA* 4.0.1 suit of programs with implemented version of UB3LYP.[68] [c]The reoptimization of the ground-state wave functions to lower-energy solutions was performed using orbital rotation. [d]It follows from EPR data for RAs that UB3LYP/def2-tzvp calculations underestimate hyperfine coupling with nitrogen nuclei; for RCs, EPR data are absent. [e]All-electron calculations with DKH-def2-tzvp basis sets[70] for C, H, N, Se and Te atoms, and SARS-DKH-def2-tzvp basis set[71] for Po atom.

The most important findings embrace reduced aromaticity of the heterocycles of **4** and **5** (NICS) and enlarged electrostatic contribution to their X–N bonds (QTAIM; X = Te, Po) as compared with **1**-**3**. Despite NICS is magnetic criterion, the aromaticity is basically thermodynamic conception[47] and reduced aromaticity (or non-aromaticity) of the heterocycles of **4** and **5** means reduced thermodynamic stabilization (*i.e.* destabilization as compared with the heterocycles of **1**-**3**) caused by perimeter delocalization of π-electrons in a π-conjugated cyclic system.

Beyond SBIs in the supramolecular context controlled by σ-holes,[6,8,11,54-61] the ground-state patterns are not enough for direct explanation of known differences in heteroatom reactivity of the title compounds. The reactivity of **1** is different from the reactivity of **2** and **3**, and, especially, the reactivity of **1**-**3** is strictly different from the reactivity of **4**.[2,4-6] For example, **1**-**3** are highly resistant against hydrolysis, whereas **4** is highly unstable towards transformation into 1,2-diaminobenzene and TeO_2 under the action of water.[4,5] This El-Nu reaction is seemingly orbital-controlled with the main contribution coming from interaction of the LUMO of electrophile (**1**-**4**) with the HOMO of nucleophile (H_2O), and minor difference in the LUMO

energies of **1**-**4** (Figure 1) cannot explain the experimental results. One can think that the reduced aromaticity of the heterocycle of **4**, *i.e.* its thermodynamic destabilization as compared with the heterocycles of **1**-**3**, facilitates access of the corresponding TS. In any way, kinetics and thermodynamics of reactions should be discussed. Furthermore, one can think that the main origin of the differences in reactivity do not regard to the properties of the ground state of unperturbed molecules of **1**-**4** but to reaction kinetics and thermodynamics where critical point may be assigned to atomic dipole polarizability of the chalcogens: as the molecules begin to interact, the electronic distribution of each one becomes polarized by the electric field of the other. For the chalcogens, the atomic dipole polarizability (au) increases with Z as *ca.* 5, 19, 29, 38 and 44 for O, S, Se, Te and Po, respectively,[76] *i.e.* by *ca.* an order of magnitude on going from O to Po. It should be emphasized that for **1**-**4** mechanisms of their heteroatom reactions are poor-studied to be a serious challenge in the field.[5] Due to obvious experimental difficulties, the main progress is expected to come from quantum chemical modeling of reaction pathways (*cf.* refs. 34,77).

Isolation of RA $[\mathbf{1}]^{\cdot-}$ and RCs $[\mathbf{1}]^{\cdot+}$-$[\mathbf{4}]^{\cdot+}$ in the form of thermally-stable salts is obvious missing link. Whereas isolation of $[\mathbf{1}]^{\cdot-}$ should not be a problem, that of $[\mathbf{1}]^{\cdot+}$-$[\mathbf{5}]^{\cdot+}$ is another serious challenge undouble worth the effort. The latter is also true for investigation of compound **1** in the context of chalcogen bonding.

Nowadays, neutral compounds **1**-**4** are, perhaps, the most interesting in the context of anion recognition via the σ-hole interactions,[57,61,78] whereas radical ions $[\mathbf{1}]^{\cdot-}$-$[\mathbf{4}]^{\cdot-}$ and $[\mathbf{1}]^{\cdot+}$-$[\mathbf{4}]^{\cdot+}$ in that of spin science[79] and AF spintronics.[80]

Acknowledgements

The authors are grateful to Dr. Alexander M. Genaev for preliminary calculations and discussions, and to the Deutsche Forschungsgemeinschaft (project no. BE 3616/6-1), the Russian Foundation for Basic Research (project no. 17-53-12057) and the Ministry of Science and Higher Education of the Russian Federation (projects nos. 4.9651.2017/BP and 0304-2017-0008) for financial support.

References

1. Chivers, T.; Laitinen, R. S. in: *Handbook of Chalcogen-Nitrogen Chemistry: New Perspectives in Sulfur, Selenium and Tellurium*, Devillanova F. A,; DuMont, W.-W., Eds., RSC Publishing, Cambridge, UK, **2013**, Vol. 1, pp. 191-237.
2. Todres, Z. V. *Chalcogenadiazoles: Chemistry and Applications*, CRC Press, Boca Raton, FL, USA, **2011**.
3. Chivers, T. *A Guide to Chalcogen-Nitrogen Chemistry,* World Scientific, Singapore, **2005**.
4. Katritzky, A. R.; Ramsden, C. A.; Scriven, E. F. V.; Taylor, R. J. K., Eds., *Comprehensive Heterocyclic Chemistry III*, Elsevier, Oxford, UK, **2008**.
5. Rakitin, O. A.; Zibarev, A. V., *Asian J. Org. Chem.* **2018**, *7*, 2397-2416.
6. Chulanova, E. A.; Semenov, N. A.; Pushkarevsky, N. A.; Gritsan, N. P.; Zibarev, A. V. *Mendeleev Commun.* **2018**, *28*, 453-460.
7. Boere, R. T.; Roemmele, T. L. *Coord. Chem. Rev.* **2000**, *210*, 369-445.
8. Pushkarevsky, N. A.; Chulanova, E. A.; Shundrin, L. A.; Smolentsev, A. I.; Salnikov, G. E.; Pritchina, E, A.; Genaev, A. M.; Irtegova, I. G.; Bagryanskaya, I. Yu.; Konchenko, S. N.; Gritsan, N. P.; Beckmann, J.; Zibarev, A. V. *Chem. Eur. J.* **2019**, 25, 806-816.
9. Neto, B. A. D.; Lapis, A. A. M.; da Silva, E. N.; Dupont, J. *Eur. J. Org. Chem.* **2013**, *2013*, 228-255.
10. Konstantinova, L. S.; Knyazeva, E. A.; Rakitin, O. A. *Org. Prep. Proc. Int.* **2014**, *46*, 475-544.
11. Cozzolino, A. F.; Elder, P. J. W.; Vargas-Baca, I. *Coord. Chem. Rev.* **2011,** *255*, 1426-1438.
12. Frisch, M. J.; Trucks, G. W.; Schlegel, H. B.; Scuseria, G. E.; Robb, M. A.; Cheeseman, J. R.; Scalmani, G.; Barone, V.; Mennucci, B.; Petersson, G. A.; Nakatsuji, H.; Caricato, M.; Li, X.; Hratchian, H. P.; Izmaylov, A. F.; Bloino, J.; Zheng, G.; Sonnenberg, J. L.; Hada, M.; Ehara, M.; Toyota, K.; Fukuda, R.; Hasegawa, J.; Ishida, M.; Nakajima, T.; Honda, Y.; Kitao, O.; Nakai, H.; Vreven, T.; Montgomery, J. A.; Peralta, J. E.; Ogliaro, F.; Bearpark, M.; Heyd, J. J.; Brothers, E.; Kudin, K. N.; Staroverov, V. N.; Kobayashi, R.; Normand, J.; Raghavachari, K.; Rendell, A.; Burant, J. C.; Iyengar, S. S.; Tomasi, J.; Cossi, M.; Rega, N.; Millam, J. M.; Klene, M.; Knox, J. E.; Cross, J. B.; Bakken, V.; Adamo, C.; Jaramillo, J.; Gomperts, R.; Stratmann, R. E.; Yazyev, O.; Austin, A. J.; Cammi, R.; Pomelli, C.;

Ochterski, J. W.; Martin, R. L.; Morokuma, K.; Zakrzewski, V. G.; Voth, G. A.; Salvador, P.; Dannenberg, J. J.; Dapprich, S.; Daniels A. D.; Farkas, O.; Foresman, J. B.; Ortiz, J. V.; Cioslowski, J.; Fox, D. J. *Gaussian 09, Revision A.01*, Gaussian Inc., Wallingford CT, **2009**.
13. Bauernschmitt, R.; Ahlrichs, R. *J. Chem. Phys.* **1996**, *104*, 9047-9052.
14. Glendening, E.; Badenhoop, D. J. K.; Reed, A. E.; Carpenter, J. E.; Bohmann, J. A.; Morales, C. M.; Landis, C. R.; Weinhold, F. *NBO 6.0.* URL: http://nbo6.chem.wisc.edu/
15. Lu, T.; Chen, F. *J. Comput. Chem.* **2012**, *33*, 580-592.
16. Lu, T.; Chen, F. *J. Mol. Graph. Model.* **2012**, *38*, 314-323.
17. URL: https://www.chemcraftprog.com/
18. Luzzati, P. V. *Acta Crystallogr.* **1951**, *4*, 193-200.
19. Suzuki, T.; Tsuji, T; Okubo, T.; Okada, A.; Obana, Y.; Fukushima, T.; Miyashi, T.; Yamashita, Y. *J. Org. Chem.* **2001**, *66*, 8954-8960.
20. Gomes, A. C.; Biswas, G.; Banerjee, A,; Duax, W. L. *Acta Crystallogr. C* **1989**, *45*, 73-75.
21. Cozzolino, A. F.; Britten, J. F.; Vargas-Baca, I. *Cryst. Growth Des.* **2006**, *6*, 181–186.
22. *The Quantum Theory of Atoms in Molecules*, Matta, C. F.; Boid, R. J., Eds., Wiley-VCH, Weinheim, **2007**.
23. Bone, R. G. A.; Bader, R. F. W. *J. Phys. Chem.* **1996**, *100*, 10892-10911.
24. Espinosa, E.; Alkorta, I.; Elguero, J.; Molina, E. *J. Chem. Phys*. **2002**, *117*, 5529-5542.
25. Reed, A. E.; Weinhold, F. *J. Chem. Phys.* **1983**, *78*, 4066-4073.
26. Reed, A. E.; Weinstock, R. B.; Weinhold, F. *J. Chem. Phys.* **1985**, *83*, 735-746.
27. Mayer, I. *Chem. Phys. Lett*. **1983**, *97*, 270-274.
28. Zibarev, A. V.; Beregovaya, I. V. *Rev. Heteroat. Chem.* **1992**, *7*, 171-190.
29. Mann, J. B.; Meek, T. L.; Allen, L. C. *J. Am. Chem. Soc.* **2000**, *122*, 2780-2783.
30. Lonchakov, A. V.; Rakitin, O. A.; Gritsan, N. P.; Zibarev, A. V. *Molecules* **2013**, *18*, 9850-9900.
31. Zibarev, A. V.; Mews, R. in: *Selenium and Tellurium Chemistry: From Small Molecules to Biomolecules and Materials*, Woollins, J. D.; Laitinen, R. S., Eds., Springer, Berlin, **2011**, 123-149.
32. Gritsan, N. P.; Zibarev, A. V. *Russ. Chem. Bull.* **2011**, *60*, 2131-2140.
33. Nian, Y.; Pan, F.; Li, S.; Jiang, H.; Feng, S.; Zhang, Y. C.; Chen, J. *Asian J. Org. Chem.* **2018**, *7*, 2285-2293.
34. Chulanova, E. A.; Pritchina, E. A.; Malaspina, L. A.; Grabowsky, S.; Mostaghimi, F.; Beckmann, J.; Bagryanskayam I. Yu.; Shakhova, M. V.; Konstantinova, L. S.; Rakitin, O. A.; Gritsan, N. P.; Zibarev, A. V. *Chem. Eur. J.* **2017**, *23*, 852-864.
35. Solodovnikov, S. P.; Todres, Z. V. *Chem. Heterocycl. Comp*. **1967**, 641-646.
36. Shundrin, L. A.; Irtegova, I. G.; Avrorov, P. A. Mikhailovskaya, T. F.; Makarov, A. G.; Makarov, A. Yu.; Zibarev, A. V. *Arkivoc* **2017**, 168-180.
37. Vasilieva, N. V.; Irtegova, I. G.; Gritsan, N. P.; Lonchakov, A. V.; Makarov, A. Yu.; Shundrin, L. A.; Zibarev, A. V. *J. Phys. Org. Chem.* **2010**, *23*, 536-543.
38. Clark, P. A.; Gleiter, R.; Heilbronner, E. *Tetrahedron* **1973**, *29*, 3085-3089.
39. Palmer, M. H.; Kennedy, S. M. F. *J. Mol. Struct.* **1978**, *43*, 33-48.
40. Hitchcock, A. P.; Dewitte, R. S.; Van Esbroeck, J. M.; Aebi, P.; French, C. L.; Oakley, R. T.; Westwood, N. P. C. *J. Electron Spectrosc. Relat. Phenom.* **1991**, *57*, 165-187.
41. Cozzolino, A. F.; Gruhn, N. E.; Lichtenberger, D. L.; Vargas-Baca, I. *Inorg. Chem.* **2008**, *47*, 6220-6226.
42. Johnstone, R. A. W.; Mellon, F. A. *JCS Faraday Trans. 2* **1973**, *69*, 1155-1163.
43. Petrachenko, N. E.; Vovna, V. I.; Zibarev, A. V.; Furin, G. G. *Khim. Geterotsikl. Soedin.* **1991**, 563-567.
44. Chen, Z.; Wannere, C. S.; Corminboeuf, C.; Puchta, R.; von Ragué Schleyer, P. *Chem. Rev.* **2005**, *105*, 3842-3888.
45. Fallah-Bagher-Shaidaei, H.; Wannere, C. S.; Corminboeuf, C.; Puchta, R.; von Ragué Schleyer, P. *Org. Lett.* **2006**, *8*, 863-866.
46. Gershoni-Poranne, R.; Stanger, A. *Chem. Soc. Rev.* **2015**, *44*, 6597-6615.
47. *Aromaticity in Heterocyclic Compounds*, Krygowski, T; M.; Cyranski, M. K., Eds., Springer, **2009**.

48. *Molecular Electrostatic Potentials: Concepts and Applications*, Murray, J. S.; Sen, K. ,Eds., Elsevier Science, **1996**.
49. Wang, H.; Wang, W.; Jin, W. J. *Chem. Rev.* **2016**, *116*, 5072-5104.
50. Kolar, M. H.; Hobza, P. *Chem. Rev.* **2016**, *116*, 5155−5187.
51. Politzer, P.; Murray, J. S. *Crystals* **2017**, *7*, 212-226.
52. Alcock, N. W. *Adv. Inorg. Chem. Radiochem.* **1972**, *15*, 1-58.
53. Scilabra, P.; Terraneo, G.; Resnati, G. *Acc. Chem. Res.* **2019**, *52*, 1313-1324.
54. Ams, M. R.; Trapp, N.; Schwab, A.; Milic, J, V.; Diederich F, *Chem. Eur. J.* **2019**, *25*, 323-333.
55. Riwar, L. J.; Trapp, N.; Root, K.; Zenobi, R.; Diederich, F. *Angew. Chem. Int. Ed.* **2018**, *57*, 17259-17264.
56. Lee, J.; Lee, L. M.; Arnott, Z.; Jenkins, H.; Britten, J. F.; Vargas-Baca, I. *New J. Chem.* **2018**, *42*, 10555-10562
57. Semenov, N. A.; Gorbunov, D. E.; Shakhova, M. V.; Salnikov, G. E.; Bagryanskaya, I. Yu.; Korolev, V. V.; Beckmann, J.; Gritsan, N. P.; Zibarev, A. V. *Chem. Eur. J.* **2018**, *24*, 12983-12991.
58. Pushkarevsky, N. A.; Petrov, P. A.; Grigoriev. D. S.; Smolentsev, A. I.; Lee, L. M.; Kleemiss, F.; Salnikov, G. E.; Konchenko, S. N.; Vargas-Baca, I.; Grabowsky, S.; Beckmann, J.; Zibarev, A. V. *Chem. Eur. J.* **2017**, *23*, 10987-10991.
59. Semenov. N. A.; Lonchakov, A. V.; Pushkarevsky, N. A.; Suturina, E. A.; Korolev, V. V.; Lork, E.; Vasiliev, V. G.; Konchenko, S. N.; Beckmann, J.; Gritsan, N. P.; Zibarev, A. V. *Organometallics*, **2014**, *33*, 4302-4314.
60. Semenov, N. A.; Pushkarevsky, N. A.; Beckmann, J.; Finke, P.; Lork, E.; Mews, R.; Bagryanskaya, I. Yu.; Gatilov, Yu. V.; Konchenko, S. N.; Vasiliev, V. G.; Zibarev, A. V. *Eur. J. Inorg. Chem.* **2012**, *2012*, 3693-3703.
61. Garrett, G. E.; Gibson, G. L.; Straus, R. N.; Seferos, D. S.; Taylor, M. S. *J. Am. Chem. Soc.* **2015**, *137*, 4126-4133.
62. Strom, E. T.; Russell, G. A. *J. Am. Chem. Soc.* **1965**, *87*, 3326-3329.
63. Marian, C. M. in: *Reviews in Computational Chemistry*, Wiley, 2001, 99-204.
64. Fedorov, D. G.; Koseki, S.; Schmidt, M. W.; Gordon, M. S. *Int. Rev. Phys. Chem.* **2003**, *22*, 551-592.
65. Kahn, O. *Molecular Magnetism*, VCH Publishers: New York, NY, USA, 1993.
66. Thirunavukkuarasu, K.; Winter, S. M.; Beedle, C. C.; Kovalev, A. E.; Oakley, R. T.; Hill, S. *Phys. Rev. B* **2015**, *91*, 14412.
67. Winter, S. M.; Oakley, R. T.; Kovalev, A. E.; Hill, S. *Phys. Rev. B* **2012**, 85, 94430.
68. Neese, F. *Wires Comput. Mol. Sci.* **2018**, *8*, e1327.
69. Wolf, A.; Reiher, M.; Hess, B. A. *J. Chem. Phys.* **2002**, *117*, 9215-9226.
70. Weigend, F. *Phys. Chem. Chem. Phys*. **2006**, *8*, 1057-1065.
71. Pantazis, D. A.; Neese, F. *Theor. Chem. Acc*. **2012**, *131*, 1292-1298.
72. Konchenko, S. N.; Gritsan, N. P.; Lonchakov, A. V.; Radius, U.; Zibarev, A. V. *Mendeleev Commun.* **2009**, *19*, 7-9.
73. Pushkarevsky, N. A.; Smolentsev, A. I.; Dmitriev A. A.; Vargas-Baca, I.; Gritsan, N. P.; Beckmann J.; Zibarev, A. V. *Manuscript in preparation*.
74. Kamada, K.; Ohta, K.; Shimizu, A.; Kubo, T.; Kishi, R.; Takahashi, H.; Botek, E.; Champagne, B.; Nakano, M. *J. Phys. Chem. Lett.* **2010**, *16*, 937-940.
75. Chivers, T.; Laitinen, R. S. *Chem. Soc. Rev.* **2015**, *44*, 1725-1739.
76. Schwerdtfeger, P.; Nagle, J. K. *Mol. Phys.* **2019**, *117*, 1200-1225.
77. Konstantinova, L. S.; Baranovsky, I. V.; Pritchina, E. A.; Mikhailov, M. S.; Bagryanskaya, I. Yu.; Semenov, N. A.; Irtegova, I. G.; Salnikov, G. E.; Lyssenko, K. A.; Gritsan, N. P.; Zibarev, A. V.; Rakitin, O. A. *Chem. Eur. J.* **2017**, *23*, 17037-17047.
78. Lim, J. Y. C.; Beer, P. D. *Chem* **2018**, *4*, 1-53.
79. Ratera, I.; Veciana, J. *Chem. Soc. Rev.* **2012**, *41*, 303-349.
80. Jungfleisch, M. B.; Zhang, W.; Hoffmann, A. *Phys. Lett. A* **2018**, *382*, 865-871.